Contents

The Effect of Alcohols on Red Blood Cell Membranes

Patric Boardman
pb449@exeter.ac.uk
Supervisor: Dr Peter. G. Petrov

April 2021

Abstract

Red blood cells were observed to undergo softening in the presence of various alcohols. The bending (κ) and shear (μ) moduli of the cell membrane reduced to $\kappa/\kappa_0 = (22.2 \pm 5.7)\%$ and $\mu/\mu_0 = (11.7 \pm 4.9)\%$ respectively after just 10 minutes upon alcoholic treatment, and barely showed significant recovery to their initial state, with a characteristic recovery timescales ranging from $\tau \sim 100 \rightarrow 500$mins. Significant variability was observed between different types of alcohol, with those having longer polymer chain lengths appearing to correlate with strong shear softening of the membrane, suggesting a potential link with *hydrophobicity*. Determining how red blood cells are affected would not only lead to a deeper understanding of the full physiological effects that alcohol has on the human body, but could also have potential applications in technologies which utilise unilamellar vesicles [1].

1 Introduction

Red blood cells (RBC) are the most ubiquitous type of blood cell. They are involved in the delivery of oxygen via the circulatory system in a wide variety of living organisms. The physical properties of its membrane are of critical importance for a plethora of specialized RBC functions [2]. Many of these are closely related to the characteristic biconcave shape of the membrane, which is adapted to maximise the uptake of oxygen [3]. Maintaining this shape is therefore of critical importance. Like many *unilamellar* vesicles, the RBC membrane is characterized by its unique mechanical properties. The mechanical parameters of relevance to the RBC are the *bending modulus* κ and the *shear modulus* μ. The value of the bending modulus is thought to be directly related to properties of the lipid bilayer [4], and it controls the extent to which the RBC can elastically deform in response to external stresses [5]. In addition to only a membrane, the mechanical properties of the RBC are also influenced by the presence of a cytoskeleton network which partially consists of a spectrin network that lines the plasma membrane. The shear modulus, μ, which parameterizes the membrane's resistance to shear stresses, becomes non zero with the additional presence of the cytoskeleton. It is thought that the value of μ is directly related to the cytoskeleton network [7]. The flexibility of the RBC allows for some remarkable biological capabilities. Such include the ability for cells that have an average radius of $\sim 4\mu$m to tunnel through much smaller blood vessels including capillaries, which

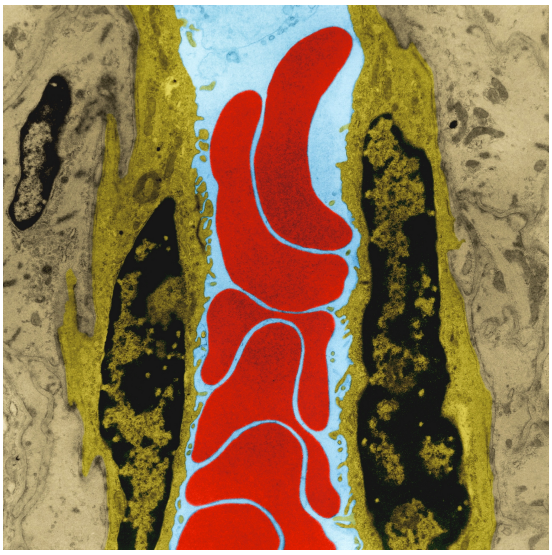

Figure 1: TEM Image of many RBC in a capillary. Credit Dennis Kunkel Microscopy, obtained from Science Photo Library [6].

have radii of ∼1 μm [8] (as shown in Figure 1). It also allows for the specialized ability to maximise their surface area to volume ratio by assuming a cigar shape which increases the efficiency in which they can release their oxygen load [9].

The interaction of short chain alcohols with the RBC membrane can provide an insight into the effects of alcohol consumption on the human body. Heavy alcohol consumption can cause a reduction in overall blood cell quantity, whilst also adversely affecting existing RBC [10]. It has been suggested that this effect is associated with haematological effects, which could then result in various medical conditions [11–14]. While it is known that alcohols have an adverse effect on the functionality of red blood cells [15], the physicals governing the interaction with the cell membrane is unclear. Alcohols are *amphiphilic* hydrocarbon molecules with an OH^- group which enables them the capability of binding and penetrating the cell membrane [16]. The amount by which an alcohol is able to do this is dependent on chain length, as longer chain alcoholic polymers are known to show greater *hydrophobicity* which results in a membrane greater penetration depth [17]. This could serve as the primary mechanism through which the mechanical properties of RBC could be affected, with molecular scale polar interactions manifesting as an observable mesoscopic change in membrane behaviour.

The objective of this analysis was to quantitatively determine whether an increase in alcoholic concentration played a role in altering specifically the mechanical properties of red blood cells. The experimental approach would rely on a previously developed technique of measuring RBC fluctuations by Hale *et al*. [18], which involved observing RBC contour fluctuations using phase contrast microscopy. By comparing variations in fluctuations before and after alcoholic treatment at regular time intervals, the relative change in κ and μ were determined. The first four molecules in the homologous series of primary alcohols were chosen for this analysis, with concentrations ranging from 0.5% to 5%. These concentrations were much larger than physiological levels observed in human blood streams after consuming typical quantities of alcohol. Typical blood alcohol concentration (BAC) can range from ∼ (0.01 to 0.4)% in the most highly extreme cases [19]. However our analysis postulates that there is an equivalence between long term alcoholic exposure at lower concentrations and short term alcoholic exposure at high concentrations, thus applicability to human physiology will still be valid.

2 Theory and Experiment

2.1 Theoretical Background

At finite temperature, RBC membranes are not static but exhibit thermal fluctuations due to thermal energy from their surroundings [20]. These fluctuations occur at length-scales of 0.1-1μm at which the presence of the cytoskeleton has a significant effect on fluctuations [21]. Static fluctuations such as these can be quantified in terms of the wavevector $\boldsymbol{q}_n$, and we aim to experimentally measure the mean squared membrane displacement $\langle\delta_n^2\rangle$ as a function of $\boldsymbol{q}_n$, such as the approach undertaken by Gov *et al*. [7]. The role of the cytoskeleton is to introduce membrane confinement, as the spectrin filaments form a connected two dimensional shell which acts to produce a restoring force on the membrane [7]. This is accounted for by modelling it as a harmonic potential with effective spring constant γ. This force distributes across the whole membrane via attachment points, which creates additional surface tension, parameterised by coefficient σ. This surface tension increases the overall value of σ more than if it was simply due to surface area conservation. As shown by Gov *et al*., [7] the total amount of free energy is given by the free energy functional:

$$E_F = \frac{1}{2}\int_S (\kappa(\nabla^2 h)^2 + \sigma(\nabla h)^2 + \gamma h^2)\,\mathrm{d}S, \quad (1)$$

where the integral is carried out over the entire surface S of the membrane. A Fourier transform was then applied to the above equation to put it in terms of the modulus of the wavevector, q. In the flat membrane approximation ($|\nabla^2 h| \ll 1$), the mean squared displacement was shown be of the form:

$$\langle\delta_q^2\rangle = \frac{k_B T}{\kappa q^4 + \sigma q^2 + \gamma}, \quad (2)$$

where $q = |\boldsymbol{q}| = \sqrt{q_x^2 + q_y^2}$ is the modulus of the wavevector, k_B is the Boltzmann constant and T is the temperature (which is assumed to be constant

at 295K). The additional γ term in the denominator results in the suppression of small wavelength modes in the fluctuation spectrum.

Experimentally, analysis of a two dimensional plane is very difficult, hence in this experiment only equatorial membrane fluctuations were monitored. In order to determine the mean squared displacement for a single line, we adopt the approach detailed in Pecreaux *et al*. [22]. By fixing the one of the coordinates (in this case y) and applying a Fourier transform to Equation (2) back into real space, the equatorial displacement was shown to be:

$$\langle \delta_n^2 \rangle = \frac{1}{2\pi} \frac{1}{\tilde{\kappa}\sqrt{\tilde{\sigma}^2 - \tilde{\gamma}}} \Bigg[\left(\tilde{\sigma} + n^2 - \sqrt{\tilde{\sigma}^2 - \tilde{\gamma}} \right)^{-1/2} - \left(\tilde{\sigma} + n^2 + \sqrt{\tilde{\sigma}^2 - \tilde{\gamma}} \right)^{-1/2} \Bigg], \tag{3}$$

where $\tilde{\kappa} \equiv \kappa / k_B T$, $\tilde{\sigma} \equiv \sigma \langle R \rangle^2 / 2\kappa$, $\tilde{\gamma} \equiv \gamma \langle R \rangle^4 / \kappa$ and $n \equiv q_x \langle R \rangle$ are dimensionless variations of these parameters. In the limit of zero confinement of the cell membrane (physically corresponding to an absence of a cytoskeleton network) Equation (3) reduces to

$$\langle \delta_n^2 \rangle = \frac{1}{2\pi} \frac{1}{\tilde{\kappa}\tilde{\sigma}} \left(\frac{1}{n} - \frac{1}{\sqrt{2\tilde{\sigma} + n^2}} \right). \tag{4}$$

The non-vanishing shear modulus of the membrane was found via perturbative treatment of the interaction between bending and shear modes. By treating any non zero contribution to the shear modulus as a perturbation, Auth *et al*. [23] showed that the shear modulus was given by

$$\mu = \frac{16\pi\kappa\sigma}{9 k_B T}, \tag{5}$$

where all symbols have their usual meanings. The relationship between the parameters given by this equation, in principle, suggests that the two parameters of interest, κ and μ, are not independent. However, the addition of the parameter σ introduces a third parameter which could mean that two of κ, σ and μ could theoretically be independent. This has been experimentally verified in previous studies, with κ and μ having been shown to account for different deformation modes [18, 24]. The precise nature in which these modes change in relation to the parameters is discussed at length in Section 2.3.

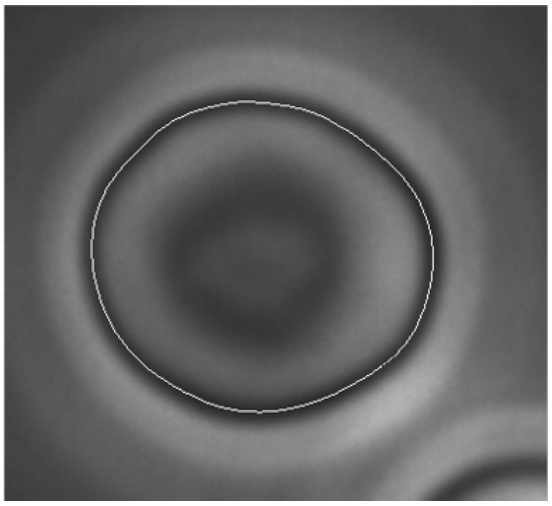

Figure 2: A phase contrast microscopy snapshot of a single cell of average radius ~ 4μm. The white line is the result of the contour extraction by virtue of the image analysis software, which corresponds to the position of the edge of the blood cell to within an uncertainty of ± 0.25% of the RBC average radius (~ 10nm). This is within typical predicted thermal fluctuation amplitudes and hence changes in this contour are assumed to be thermally driven [26].

2.2 *Contour Fluctuation Detection*

Visualization of the cell membrane fluctuations was carried out using a phase contrast microscopy system, outlined by Hale *et al*. [24]. Video sequences were recorded for each cell sample at regular time intervals at a typical frame rate of 60fps (Moticam 2000 2 MP progressive scan digital video camera). For each cell in the sample, the coordinates of the equatorial contour were extracted using a computational sub pixel resolution algorithm [25]. In summary, the algorithm scanned certain pixel rows and columns of each image which were specified manually by dragging a bounding box over each RBC. By locating positions which had an intensity minimum, this has a direct correspondence to the position of the cell edge. Due to the fact that amplitude fluctuations are relatively small in comparison to the size of the cell, the algorithm was able to average the coordinate points over all frames to produce the sub-pixel resolution of the contour. A visual representation of this approach is given in Figure 2. Once the coordinates were extracted, the Cartesian coordinates were converted into polar coordinates (r, θ) with the cell centre at the origin. The variation in absolute distance between each point along the

contour and the centre were then decomposed into a series of Fourier harmonics [22] with mode number $n = q\langle R\rangle$ (with $\langle R\rangle$ the average cell radius)

$$r(\theta) = \langle R\rangle\left\{1 + \sum_n \left(a_n \cos(n\theta) + b_n \sin(n\theta)\right)\right\}$$

where theoretically the summation occurs over every possible mode. Of particular importance are the Fourier weighting coefficients a_n and b_n which are defined in the usual way [27]:

$$a_n = \frac{1}{2\pi}\int_0^{2\pi} r(\theta)\cos(n\theta)\,\mathrm{d}\theta$$

$$b_n = \frac{1}{2\pi}\int_0^{2\pi} r(\theta)\sin(n\theta)\,\mathrm{d}\theta$$

It is these quantities that were to be extracted from the contour in the polar coordinate representation. For a given cell, each video frame will have unique dependence of a_n and b_n on mode number n. These coefficients have a certain value depending on how common they are in the RBC contour when decomposed into a Fourier series (i.e for a cell with small wavelength fluctuations coefficients with higher n will have a greater value than those with low n.) We then took an average of a_n and b_n over all frames for a given measurement of a given contour, and then combined to give the mean squared displacement $\langle\delta_n^2\rangle = (\langle a_n^2\rangle - \langle a_n\rangle^2) + (\langle b_n^2\rangle - \langle b_n\rangle^2)$. This quantity is of particular importance as it is directly related to the mechanical parameters κ, σ and γ through Equation (3).

Experimentally it was shown by Hale *et al.* [18] that modes up to $n \approx 18$ can be reliably detected using this method. However, higher-order modes were shown to be greatly affected by the optical resolution and camera noise. In this analysis though, this does not appear to be an issue as it has been shown that modes in this regime do not have a significant effect on the mechanical parameters [24].

2.3 Spectral Analysis and Fitting

The characteristic dependence of $\langle\delta_n^2\rangle$ on the mode number n has previously been shown across multiple studies [7, 18, 23, 24, 28] to be directly influenced by the mechanical parameters. The precise nature as to how each parameter influences the fluctuation spectrum was qualitatively shown by varying each parameter in Equation (3). This is illustrated in Figure 3.

An increase in the bending modulus κ has the effect of shifting values for the mean squared displacement globally downwards for all n. An increase in both the surface tension σ and the confinement potential γ appears to have a more complex effect on the overall spectrum. It is clear that the lower order modes experience the greatest shift in response to a increase in either σ or γ, with σ producing the greatest effect. By contrast a discrepancy is observed for higher order modes between an increase in σ and γ. Spectral lines appear to bunch together for higher order modes upon an increase in γ, whereas an increase in σ shifts these lines further down. In our experiment, we compared these spectra shown in Figure 3 (which simply originate from Equation (3)) with ones produced through our experimental analysis, which enabled extraction of κ, σ and γ. Explicit extraction of these parameters involved the use of the Levenberg–Marquardt algorithm [29]. In essence, fluctuation spectral data obtained were initially fitted with Equation (4) using a non linear least squares fitting procedure, from which the values of κ and σ were extracted. These values were then used as initial guesses in the three parameter fitting procedure, which fitted the obtained data with Equation (3) in order to find the values of κ, σ and γ which minimised data residuals. The shear modulus μ was then found via Equation (5).

2.4 Uncertainties and Limitations

As discussed in previous studies which implement the same experimental technique [18, 24], we acknowledge some essential limitations in our approach. As per the shallow gradient assumption made in order to reconcile the well known result given in Equation (2), this analysis can only legitimately be used if fluctuation wavelengths are much less than the cell radius ($\lambda \ll R$). The lower order modes in this experiment however have wavelengths that are comparable to the cell radius ($\lambda \sim R$), hence vesicles that are not quasi-circular would theoretically have a large impact on the wavelengths. Pécréaux *et al.* [22] however showed that fluctuations are almost entirely independent of geometry for mode numbers greater than $n = 3$, which spans almost the entire domain of n that is of relevance to the experiment. Since most RBC analysed in this experiment were quasi-circular

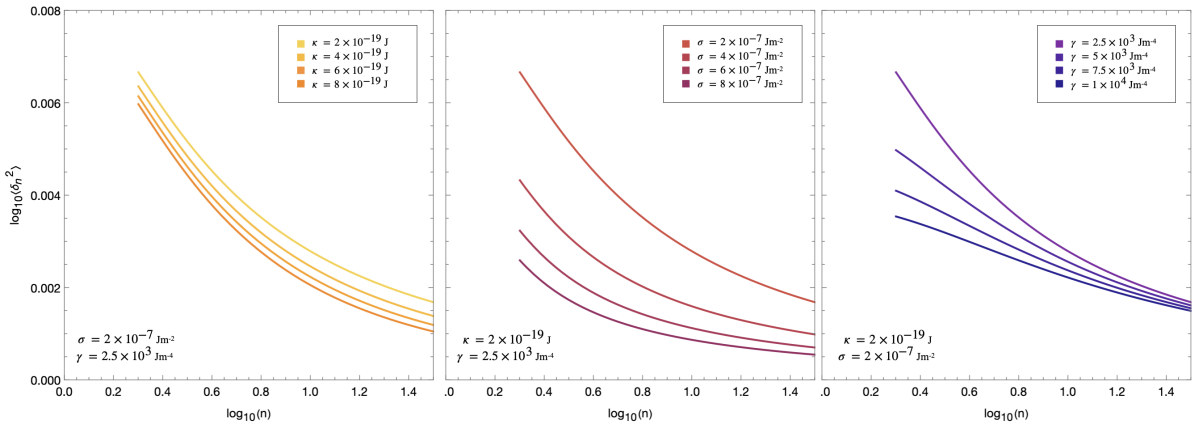

Figure 3: (Reproduction of Figure 1 from Hale *et. al* [18]) Fluctuation spectra in the logarithmic representation showing the influence of changing bending modulus κ, surface tension σ and confinement potential γ on the characteristic curve. *Left*: Effect of increasing κ ($\kappa = 2{\times}10^{-19}$J, $4{\times}10^{-19}$J, $6{\times}10^{-19}$J, $8{\times}10^{-19}$J), ($\sigma = 2{\times}10^{-7}$Jm^{-2}, $\gamma = 2.5 \times 10^{3}$Jm^{-4}). *Middle*: Effect of increasing σ ($\sigma = 2{\times}10^{-7}$Jm^{-2}, $4{\times}10^{-7}$Jm^{-2}, $6{\times}10^{-7}$Jm^{-2}, $8{\times}10^{-7}$Jm^{-2}), ($\kappa = 2 \times 10^{-19}$J, $\gamma = 2.5 \times 10^{3}$Jm^{-4}). *Right*: Effect of Increasing γ ($\gamma = 2.5{\times}10^{3}$Jm^{-4}, $5{\times}10^{3}$Jm^{-4}, $7.5{\times}10^{3}$Jm^{-4}, $1{\times}10^{4}$Jm^{-4}), ($\kappa = 2 \times 10^{-19}$J, $\sigma = 2 \times 10^{-7}$Jm^{-2}).

this would result in negligible uncertainties in measurements of $\langle \delta_n^2 \rangle$ even for low order modes.

The phase contrast microscopy method of RBC contour detection ultimately relies on a computational algorithm to automatically locate the coordinates of the contour, which introduces an additional source of systematic error [25]. In essence, the exact location of the contour is undetermined using this method. However, it has been observed across numerous studies implementing this technique that there is a characteristic feature of the phase contrast microscopy method, which is a sharp ring of minimal intensity around the RBC. It is this ring that the contour detection algorithm is detecting in each frame. By evaluating the relative change in the position of the ring across all frames during a particular measurement, this is assumed to have a direct correspondence to the changes in positions of the contour. In addition to this, these positions are never observed to change largely between adjacent frames, as through observation RBC do not show any significant bulk motion. It can therefore be assumed that changes in the detected ring found by the image analysis software are the direct result of thermal fluctuations.

It is worth mentioning that because of lab inaccessibility (due to the COVID-19 pandemic) all recordings of RBC fluctuations were obtained prior to this analysis, and unfortunately there appear to be measurement omissions, particularly at larger concentrations for butanol (none at $c > 2\%$) and propanol (none at $c > 3\%$). Despite this, we are still able to observe trends and conduct quantitative analysis from the available data.

3 Results

3.1 *Pre-treatment Analysis*

Figure 4 shows a typical fluctuation spectrum obtained following our experimental procedure, which is highly representative of the majority of all the cells we analysed. The data in Figure 4 shows that there is an exponential relationship between the mode number n and the mean squared displacement $\langle \delta_n^2 \rangle$ before treatment, as expected. For values of n above ~ 6, the data points appear to follow a power law dependence of $n^{-4.34}$. This favourably compares to the well known n^{-4} power law (shown by the red dotted line) for confinementless, bending dominant membranes. However, a large deviation is observed for lower order mode numbers, which suggests that there is additional membrane surface tension and/or confinement, as predicted. This deviation for lower order modes is in exact agreement with many previous studies [18,23,24,28] and has been comprehensively analysed. Their findings show that the closed topology coupled with the addition of the cytoskeleton network of the membrane results in the suppression of these lower or-

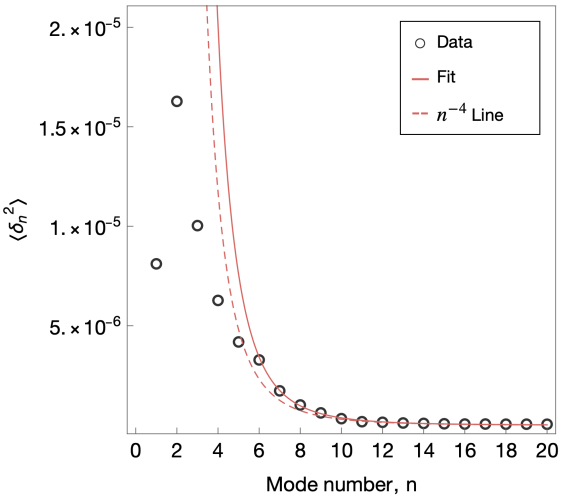

Figure 4: Experimentally obtained fluctuation spectrum of a typical pre-treated RBC (data points shown as open circles) in the linear representation. The filled line is a functional fit of the data neglecting modes $n = 1 \rightarrow 6$. The fitting function taking the form An^{-k}, where A (units m^2) is a constant and k is the power dependence, and has a value for this spectrum of 4.34. The dotted line represents the well known n^{-4} power law determined from previous experiments.

der modes, with the additional confinement created by the network being found to have the greatest effect [7]. The consistency of our findings with previous studies show that these spectra are sufficient to be used to determine the values of the moduli pre-treatment.

We obtain an average value for the bending modulus across all untreated cells of $\langle \kappa_0 \rangle = (6.5 \pm 1.0) \times 10^{-19}$J. This value corresponds well with values obtained in previous experiments implementing a similar technique, with Hale *et al.* [18, 24] measuring values typically within the range of $(2 - 7) \times 10^{-19}$J. This value also compares well with those obtained through a different experimental technique, which typical values of 1.8×10^{-19}J obtained by Selvan *et al.* [30] and $1. \times 10^{-19}$J and 3.3×10^{-19}J obtained by Frohlich *et al.* [31]. The average value for the membrane shear modulus prior to treatment was found to be $\langle \mu_0 \rangle = (8.5 \pm 1.9) \times 10^{-4}\text{Nm}^{-1}$. This value is also very comparable with the values obtained by Hale *et al.* [18, 24]. However, it has somewhat more significant discrepancies of $\sim 10^2$-10^4 with other studies which implement a different experimental technique. Hénon *et al.* used optical tweezering to extract a value for the shear modulus of $(2.5 \pm 0.4) \times 10^{-6}\text{Nm}^{-1}$, while Lee *et al.* used micropipetting to extract a value of $(5.5 \pm 3.3) \times 10^{-6}\text{Nm}^{-1}$. The deviation that occurs using this technique has been comprehensively discussed by Hale *et al.* and occurs due to the long wavelength modes given by Equation (3). The values of both κ and μ in our experiment were all found to be within the regimes given by the uncertainties of the average values, hence this discrepancy in $\langle \mu_0 \rangle$ can be attributed to the experimental method. Our analysis however focuses on how both moduli change relative to pre-treatment. Because of this, we display our results as relative fractional changes κ/κ_0 and μ/μ_0, which eliminates this particular issue.

3.2 *Post Treatment Analysis of the Fluctuation Spectrum*

We now draw comparisons between how the fluctuation spectrum is affected upon treatment of the four alcohols, compared to pre-treatment. Spectra of a typical RBC treated with 1% butanol is shown in Figure 5. We observe that for this particular cell the fluctuation spectra appear to have been upwards shifted across the entire mode domain. This is most apparent in the logarithmic representation (shown in Figure 5b) where we observe that linear trends found through fitting have been shifted upwards. The greatest shift in $\langle \delta_n^2 \rangle$ occurs after 10 minutes post-treatment (shown by the yellow points in Figure 5), after which fluctuations return somewhat closer to their pre-treatment values, although even after 90 minutes (shown by the darker green points in Figure 5), $\langle \delta_n^2 \rangle$ is still observably higher than for pre treatment. By reconciling the fluctuation spectrum shown in Figure 5 with the theoretical fluctuation spectra shown in Figure 3, we can deduce which of the respective moduli were most affected. In this particular case, it is apparent that higher order modes have undergone a more significant upwards shift in $\langle \delta_n^2 \rangle$ than the lower order modes. This is best illustrated in the logarithmic representation (Figure 5b), where we observe decreases in the gradients of the fitting functions (k) for at each time ($k \sim (4.34, 4.57, 4.02, 3.64)$ for $t = 0, 10, 30, 90$ mins respectively). This would suggest that the bending modulus κ decreased more significantly than both σ and γ, indicative of a softening of the lipid bilayer of the RBC. Indeed, the relative values obtained for the three parameters κ,

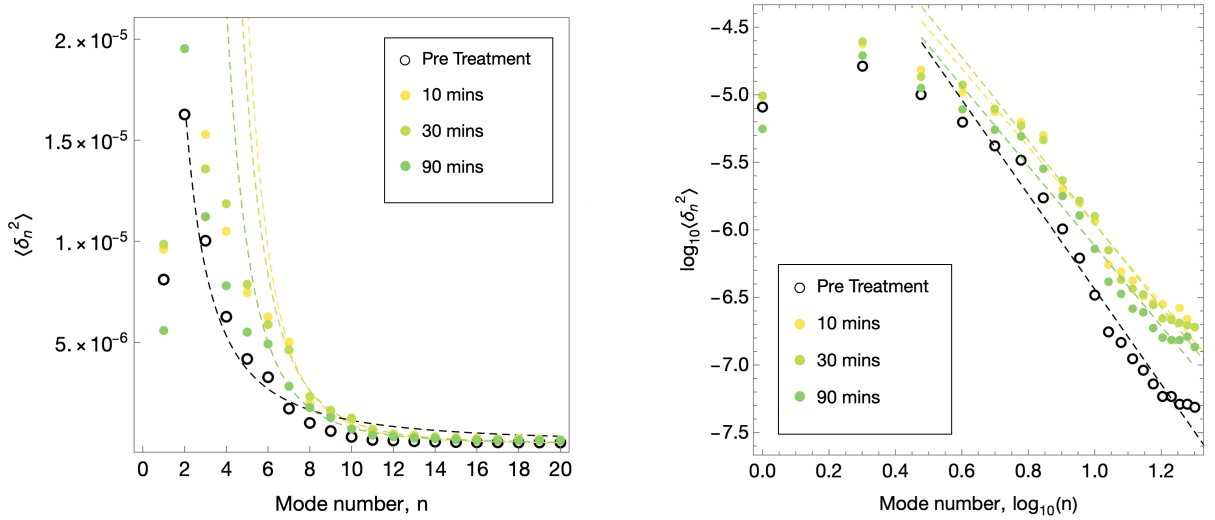

(a) Contour fluctuation spectrum in linear representation, with exponential decaying functional fits of form An^{-k} (where A (units m^2) and k (dimensionless) are fitting coefficients which fit all data points consisting of $n > 6$) shown as dotted lines (values given in Section A.2).

(b) Contour fluctuation spectrum in logarithmic representation, with linear fitting functions of the form $\log(A) - k\log(n)$ (where A and k are fitting coefficients which fit all data points consisting of $n > 6$) shown as dotted lines (values given in Section A.2)

Figure 5: Contour fluctuation spectra of RBC treated with 1% butanol shown on both a linear scale (left) and a logarithmic scale (right). Untreated cells are shown as open black circles, while values at varying times after treatment are shown as different coloured circles. The dotted lines are statistical models fitted to the various data, and show that the data follows an exponentially decreasing trend, with average observed dependence $\langle \delta_n^2 \rangle \propto n^{-(4.1\pm0.5)}$. In both Figure 5a and Figure 5b modes $n = 1 \rightarrow 6$ were omitted from the fitting function as these modes were already shown to deviate from the n^{-4} power dependence).

σ and γ of this particular cell after $t = 10$ mins are $\kappa/\kappa_0 = (39.9 \pm 6.4)\%$, $\sigma/\sigma_0 = (61.9 \pm 1.3)\%$ and $\gamma/\gamma_0 = (96.0 \pm 4.0)\%$. By performing a similar analysis on many different cells, we found that this particular characteristic shift in bending modes did *not* occur for all blood cells. In an attempt to overcome this, we analyse multiple blood cells in the same sample, and perform averaging. We acknowledge that the variability we observe within in cell samples is a limitation of this approach, and hope that by analysing a large number of cells we can deduce the overall trends.

3.3 *Time Dependence*

The relative changes in both bending and shear moduli (κ/κ_0) and (μ/μ_0) were measured for many different concentrations for the first four alcohols in the standard homologous series. At first, we compared how the four different alcohols affected the cells over time at a fixed concentration. A plot of these results is shown in Figure 6. From Figure 6, a common trend is observed between all four alcohols at 1% concentration, namely a significant decrease in both the bending and shear moduli in the first 10 minutes after treatment, after which a slow recovery towards their initial values appears to take place. The percentage change for each alcohol after 10 minutes κ/κ_0 = 68.9±10.3, 63.6±12.7, 53.6±8.5 and 49.7±5.3 and μ/μ_0 = 70.0±13.0, 66.9±19.3, 37.6±8.5 and 35.4±5.4 for methanol, ethanol, propanol and butanol respectively (all values are given as a fractional percentage of the moduli pre-treatment). After this a gradual recovery is observed in both moduli, which tends towards pre-treatment values, although there is variability in the extent to which this happens.

By drawing comparison between alcohols, it is clear that in the short term, alcohols with longer chain length exhibit a greater relative change in both moduli. The values of κ/κ_0 and μ/μ_0 for the longest chain alcohol, butanol after 10 minutes are (49.7±5.3)% and (35.4±5.4)% respectively. This compares with the moduli values of shortest chain alcohol methanol, which are (68.9±10.3)% and (70.0±13.0)% For measurements in the longer term, the effect of chain length on the recovery both

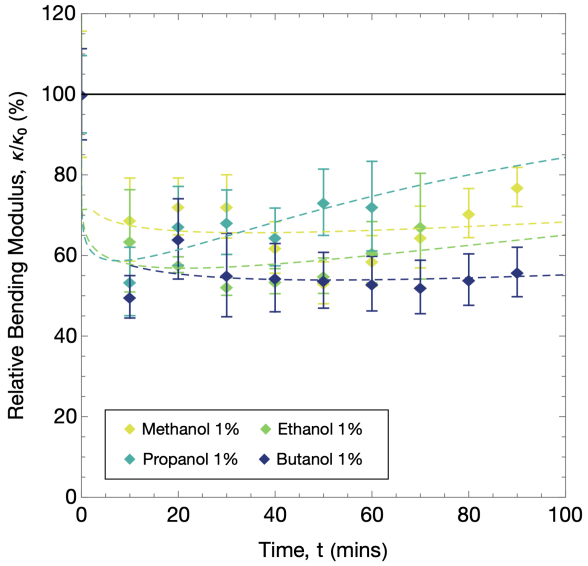

(a) Time dependence of the relative bending modulus κ/κ_0.

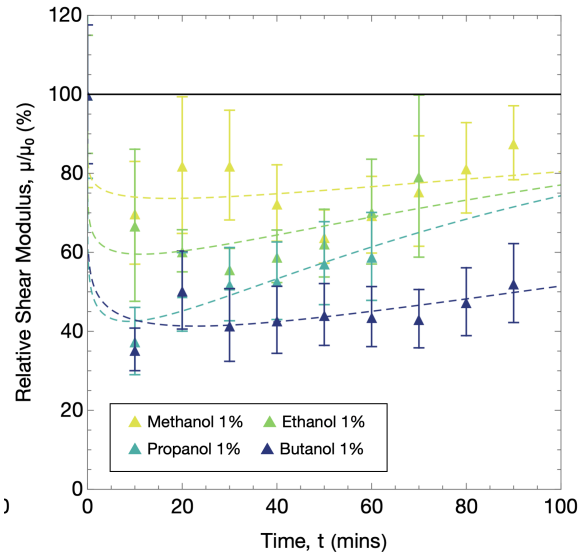

(b) Time dependence of the relative bending modulus μ/μ_0.

Figure 6: Time dependence of both relative bending and shear moduli for all four alcohols at 1% concentration by volume. The dotted lines are both fitting functions of the form $f(t) = 100 - At^k e^{-t/\tau}$, where A (units mins^{-k}), k (dimensionless) and τ (units mins) are fitting coefficients determined via non linear regression analysis (Full values given in Section A.2).

moduli is less clear, in particular for the relative bending modulus κ/κ_0 as crossing between trendlines for each alcohol is observed. The values for butanol remain much lower compared to the values for the other alcohols even after long times (κ/κ_0 = (55.9±6.1)%, μ/μ_0 = (52.2±10.0)% at t =90 mins). We also draw comparison between the relative changes of the elastic moduli across all alcohols. The largest relative change occurred in the shear modulus upon treatment with butanol after just 10 minutes (μ/μ_0 = (35.4±5.4)%), after which recovery takes place but at a relatively slow rate (time recovery constant $\tau \sim$ 120mins from fit). By comparison the value for the relative change in bending modulus is κ/κ_0 = (49.7±5.2)%, which indicates that in the case of butanol treatment, the shear modulus is more greatly affected than the bending modulus, although both show a significant decrease compared to baseline. This is also true in the case of propanol (κ/κ_0 = (53.6±8.5)%, μ/μ_0 = (37.8±8.5)% at t = 10mins). The effect does not appear to be as apparent in the case of the other two alcohols, with the relative change in shear modulus for methanol in particular not appearing to drop to values significantly lower than that of the relative bending moduli (at t =10mins, κ/κ_0 = (68.8±10.3)%, μ/μ_0 = (70.0±13.0)%). The overall effect of chain length appears to have more of an impact on μ/μ_0. This would indicate a greater potency for longer alcohol chains to not only have a greater overall impact, but to have a greater impact on the shear modulus of the membrane and hence effect on the cytoskeleton network.

Justification for the functional fit of the form:

$$f(t) = 100 - At^k e^{-\frac{t}{\tau}},$$

given in Figure 6 comes from the assumption that over large timescales, both moduli will return to (or very close to) their initial values prior to treatment. A functional model of this form assumes that there is no external influence that would affect RBC fluctuations and hence their respective moduli after treatment. Figure 6 shows that the functional fit appears to lie within the uncertainty region of most of the points, the exception being some of these methanol values that occur in both bending and shear modulus, which lie below the lower uncertainty bound for both κ/κ_0 and μ/μ_0.

3.4 *Concentration Dependence*

The concentration dependence of both elastic moduli at a fixed time of t = 10 mins averaged across all cells is shown in Figure 7. In this analysis we

measure concentration as a fractional percentage by volume of alcohol in the water solvent. The data shown in Figure 7 show qualitatively that an increase in alcoholic concentration results in a reduction in both κ/κ_0 and μ/μ_0 for all types of alcohol. The most extreme change in the bending modulus κ occurs in methanol ($\kappa/\kappa_0 = (22.2 \pm 5.7)\%$) at $c = 3\%$ and that of the shear modulus μ also occurs in propanol ($\mu/\mu_0 = (11.7 \pm 4.9)\%$) also at $c = 3\%$. Drawing comparison between alcohols, we observe that the relative change in both κ and μ after 10 minutes is highly comparable between methanol and ethanol, with both fitted functions almost overlapping (for κ/κ_0, concentration decay constant $\lambda = 0.250$, 0.278 and for μ/μ_0, $\lambda = 0.285$, 0.290 both for methanol and ethanol respectively). Similarly, propanol and butanol also exhibit pairing in their effect on κ and μ trendlines (κ/κ_0, $\lambda = 0.566$, 0.562 and for μ/μ_0, $\lambda = 0.950$, 0.915 both for propanol and butanol respectively). However, between these two pairs of trend lines there appears to be a significant difference. This leads to the observation that longer chain alcohols have a greater effect on the moduli, although this observation does not hold for all measured concentrations (eg. $\kappa/\kappa_0 = (47.9 \pm 5.3)\%$ for propanol and $\kappa/\kappa_0 = (63.7 \pm 7.4)\%$ for butanol both at $c = 0.5\%$). We now draw general comparison between how the respective moduli change depending on alcoholic concentration. The most significant change occurs with the relative shear modulus, with an near tenfold drop occurring in propanol at a concentration $c = 3\%$ ($\mu/\mu_0 = (11.7 \pm 4.9)$ %), after just 10 minutes of treatment. The corresponding value for the bending modulus change at the same concentration for the same alcohol is $\kappa/\kappa_0 = (25.7 \pm 6.1)\%$. This is, in fact, representative of all data analysed, with greater changes observed in the shear moduli with respect to the corresponding bending moduli. In accordance with temporal observations of the elastic moduli from Figure 6, the data from Figure 7 show that in addition to an overall softening of the membrane, it is the shear modulus μ that appears to have been affected more significantly than the bending modulus κ. The exponential fitting function of the form:

$$f(c) = 100e^{-\lambda c},$$

assumes that for small concentrations, κ/κ_0 and μ/μ_0 decrease linearly with c (*c.f* taylor expansion $e^{-x} \approx 1 - x$). For concentrations much larger than those we use for this experiment, RBC are expected to become highly softened and thus highly denatured, resulting in near zero values for κ and μ. In this limit, the membrane approaches becoming a two dimensional fluid and deformations become irreversible. For the available data, Figure 7 shows the fitting function appears to fall within the uncertainty regime for the majority of data, with the exceptions mostly occurring in propanol and butanol values for κ/κ_0 and μ/μ_0 at 0.5% concentration (largest deviation from 0.5% propanol in κ/κ_0 at $\sim$ 27.5%). This would lead to the suggestion that alcohols, even in small amounts cause significant softening and the effect becomes satured more quickly than the model would suggest. Accessibility to further data could potentially lead to a more accurate determination of the empirical dependence of κ/κ_0 and μ/μ_0 on c, however our functional fit is observed to correspond reasonably well to most of the data.

3.5 Cell Radius Change

A general enlargement was observed across all cells upon alcoholic treatment. This effect is shown in Figure 8, where cell radius $\langle R\rangle/\langle R_0\rangle$ is shown as a function of both time and concentration. The data show that for all alcohols there is an observed enlargement of the cell radius, with the greatest observed change being that of propanol at $c = 3\%$ with a fractional increase of $\langle R\rangle/\langle R_0\rangle = 1.09 \pm 0.80$. However, at fixed alcoholic concentration, the data from Figure 8a shows that over time and averaged across all cells, ethanol was observed to have a slightly more significant impact on radius. Despite this, there appears to be little difference between other alcohols, and any small differences are not significant enough for them to not be caused by measurement uncertainties. Therefore, there is little evidence to suggest that the type of alcohol has any association with radius. In terms of the recovery towards initial cell radius, this does not appear to take place over the timescales in this experiment. The fitting constant τ (which is indicative of a recovery timescale) is on the order of $\sim 150 \rightarrow 1000$mins, which is far greater than the time scope of this experiment. This leads to the suggestion that RBC membrane may not make a full recovery towards its initial radius if alcoholic

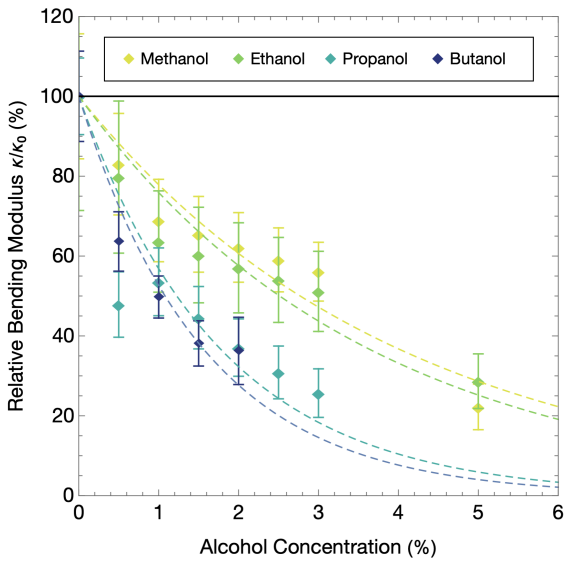

(a) Concentration dependence of the relative bending modulus κ/κ_0.

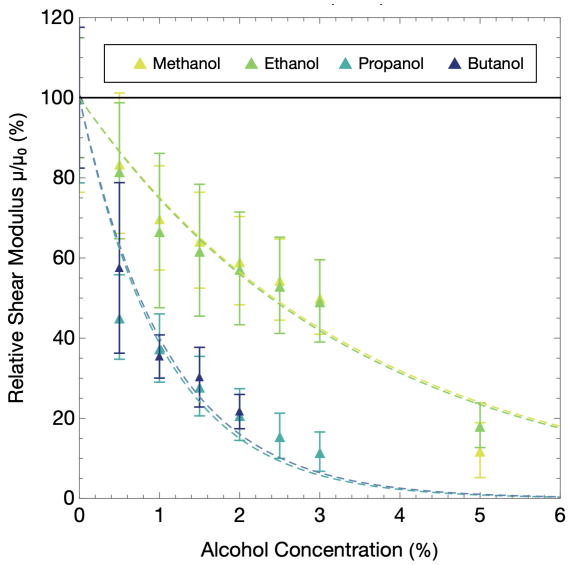

(b) Concentration dependence of the relative bending modulus μ/μ_0.

Figure 7: Concentration dependence of both relative bending and shear moduli for all four alcohols at fixed time t = 10mins. The dotted lines are both fitting functions of the form $f(c) = 100e^{-\lambda c}$, where λ is a (dimensionless) fitting coefficient determined through a non linear fit (Full values given in Section A.2).

presence continues. The data from the concentration dependence given in Figure 8b, shows that for larger concentrations, there appears to be a larger increase in radii after just 10 minutes. As with the data given as a function of time, there appears to be no significant differences observed between alcohols. The observation that the changes in cell radius are independent of alcohol is in contrast with that of the two relative bending moduli, where there was some evidence to suggest an association. This suggests that the mechanism that increases the cell radius is potentially independent of the direct interaction between alcohols with the membrane. Further experimental analysis could potentially lead to insights as to the nature of why this effect occurs.

3.6 *Hydrophobicity*

Our analysis so far has produced the observation that there appears to be an association between the potency of the alcoholic polymer to affect the RBC membrane, and the type of alcohol used in treatment. Specifically, the data from Figure 6 and Figure 7 show that longer chain primary alcoholic polymers are correlated with an increased reduction in the relative bending moduli. A potential explanation is in relation to the hydrophobicity, which is commonly characterised by the quantity $\log(P)$, where P is typically referred to as the *n-octanol-water partition ratio* [32]. The value of $\log(P)$ is positive for hydrophobic substances and negative for hydrophilic substances.

To analyse a potential association, we refer to the work conducted by Hansch *et al.* [33], where they experimentally measured the values of $\log(P)$ for all primary alcohols. These values of the hydrophobicity are given in Table 1. The values of $\log(P)$ from Table 1 indicate that the two shorter chain alcohols, methanol and ethanol were hydrophilic whilst propanol and butanol were hydrophobic; although all values were within the range $-1 < \log(P) < 1$. It was nevertheless shown by Ly *et al.* [17] that this small change in polymer length results in a significant difference in membrane penetration by the alcoholic polymer molecules, hence indicating a high susceptibility the membrane has to hydrophobicity. It was then determined by Sonméz *et al.* (2013) [2] that longer chain alcoholic polymers are correlated with significantly greater levels of haemolysis. To determine if this is reflected in the mechanical properties, we draw comparison between hydrophobicity and the relative change in both moduli using our data. This is shown in Figure 9. The data in Figure 9 suggests a potential association between the hydropho-

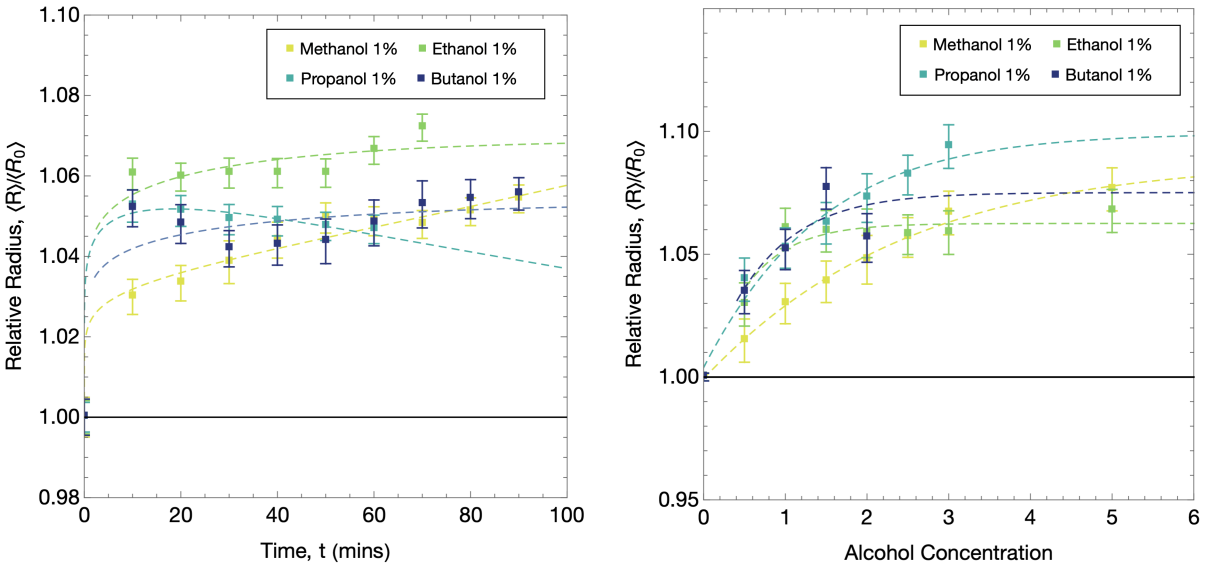

(a) Time evolution of the fractional increase in cell radius $\langle R\rangle/\langle R_0\rangle$ for all four alcohols a fixed concentration of 1%. The dotted lines are functional fits of the form $f(t) = 1 + At^k e^{-\frac{t}{\tau}}$, where A (units mins^{-k}), k (dimensionless) and τ are fitting coefficients obtained through a non linear fit (full values given in Section A.2).

(b) Concentration dependence on the relative cell radius $\langle R\rangle/\langle R_0\rangle$ at fixed time of t = 10mins. The dotted lines are functional fits of the logistic sigmoid form $f(c) = A(1/2 + (1 + \exp(-\lambda c + \delta))^{-1})$ where A (units m), λ and δ (both dimensionless) are fitting coefficients obtained through a non linear fut (full values given in Section A.2)

Figure 8: Relative fractional increase in cell radius $\langle R\rangle/\langle R_0\rangle$ as a function of both time (a) and concentration (b). The dotted lines are functional fits that arise from assumptions about $\langle R\rangle$ in the limits of large t (for (a)) and large c for (b). In the case of (a) we assume that for large t, $\langle R\rangle/\langle R_0\rangle \to 1$ and the cell recovers its original radius. In the case of (b), we assume that in the limit of large c, there is no longer an increase in $\langle R\rangle/\langle R_0\rangle$.

Alcohol	Formula	Structure	log(P)
Methanol	CH_3OH	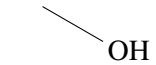	-0.77
Ethanol	C_2H_5OH	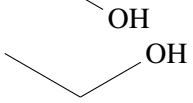	-0.31
Propanol	C_3H_7OH		0.25
Butanol	C_4H_9OH	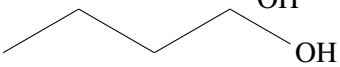	0.88

Table 1: Table showing chain lengths and log(P) values of the alcoholic polymers used in this study, adapted from [33].

bicity and the relative changes in κ and μ. As the hydrophobicity increases, both relative moduli appear to show a decrease, which is in accordance with our previous findings. Of particular interest is the relative difference in moduli between the two short chain alcohols and the two longer chain alcohols, which was also one of our previously discussed findings shown in Figure 7. This suggests that even slight deviations in hydrophobicity correspond to differences between the relative changes in elastic moduli, hence verifying the observation found by Ly *et al.* [17] of the membrane being highly susceptible to changes in the hydrophobicity. Having said this, even the alcoholic polymers that would be classified as hydrophylic (log(P) = -0.77, -0.31 for methanol and ethanol) still correspond to a reduction in both moduli, albeit to a lesser extent. In terms of how each of the moduli were affected, it is the shear modulus μ that appears to have been much more greatly effected in the hy-

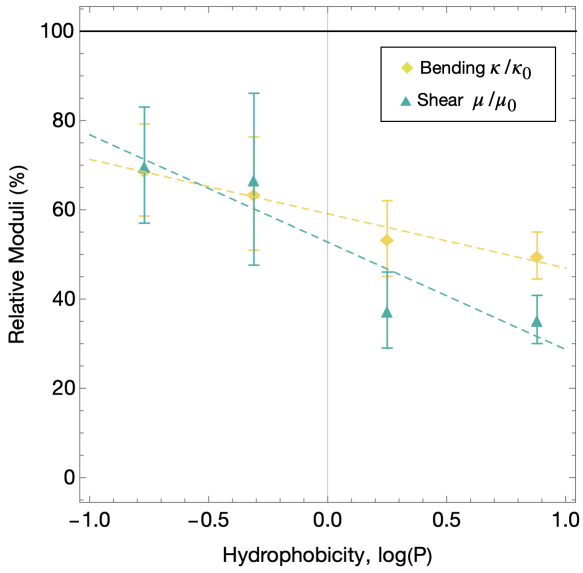

Figure 9: Association between hydrophobicity and the relative moduli κ/κ_0 and μ/μ_0 (data points shown as yellow diamonds and turquoise triangles respectively), all at t = 10mins and c = 1%. The dotted lines are fitting functions of the form $A + B\log(P)$ where A and B are (dimensionless) fitting coefficients determined through non linear fit (full values given in Section A.2).

drophobic regime ($\log(P) > 0$) than the respective relative change for the bending modulus κ. In the case of propanol, for example, ($\log(P) = 0.25$), the relative changes are (53.6±8.5)% and (37.5±8.5)%, for κ/κ_0 and μ/μ_0 respectively. By contrast, no appreciable difference is observed between κ/κ_0 and μ/μ_0 in the hydrophilic regime, with the relative change in the case of methanol ($\log(P) = -0.77$) being (68.9 ± 10.3)% and (70.0 ± 13.0)% for κ/κ_0 and μ/μ_0 respectively. We therefore suggest that the hydrophobicity primarily has modes that correspond to a change in the spectrin network, although we do not neglect the appreciable shift in modes corresponding to the lipid bilayer. We observe similar trends at other concentrations at different times. However, due to restricted dataset the data alone is insufficient to claim a direct relationship between hydrophobicity and both moduli. Despite this, the relationship between hydrophobicity and the moduli does bear resemblance with the findings of Sonméz *et al*. [2] (2013) where they observed stark differences between the same four alcohols in the observed haemolysis.
The fitting function of the form:

$$f(\log(P)) = A + B\log(P),$$

was chosen due to the decreasing trend observed in Figure 9. By virtue of the work from McKarns [34] *et al*. (1997), we know that the hydrophobicity of alcohols increases linearly with with the number of carbon atoms in the chain, and thus we expect moduli values to be reduced further. While this model takes into account hydrophobicity, it does not account for other physical factors that could affect the elastic moduli, including the viscosity and of the alcoholic solution.

4 Discussion

4.1 *Association with Hydrophobicity*

The results we obtain are overall indicative that the presence of alcohols has an association with the mechanical properties of the RBC. Both the relative bending and shear moduli were shown to reduce upon alcoholic treatment, which provides evidence that softening of the membrane occurred in both the lipid bilayer and the cytoskeleton network. In particular, for treatment with alcohols which had a greater hydrophobicity, it was the shear modulus which underwent the greatest fractional decrease, thus possibly alluding to a greater softening of the membrane spectrin network. This result could be understood in terms of the molecular interaction that takes place between alcohol polymer molecules and the bilayer. The nature of the semi-permeability of the membrane would imply that longer chain alcoholic polymers are less likely to transport freely across the membrane, and are more likely to bind with the hydrophobic membrane core. With the additional presence of these alcohols in the core, the electrostatic interactions between phospholipid molecules become screened, which leads to a more deformable membrane. While this would still cause a significant reduction in bilayer elasticity, the hydrophobicity of these alcohols is likely to have significant impact on the spectrin network due to the screening effect. The comparable sparse geometry of the spectrin network could potentially be highly susceptible to polarity changes within the bilayer, causing a significant reduction in confinement strength. This could possibly serve as the driving mechanism behind consistent observations [2, 17] that hydrophobic alcohols affect deformability and fluidity to a greater extent than hydrophilic ones.

4.2 Timescales of Possible Recovery

The observed softening of the RBC membrane occurring at timescales of less than 10 minutes after alcoholic treatment shows that the effect is relatively short term. For all alcohols, the recovery of both κ and μ was slow and even after 90 minutes, no full recovery was observed. While an initial assumption is that both moduli recover eventually, further observational data is necessary to experimentally determine whether this happens. For timescales up to 90 minutes however, the bending and shear modulus of RBC becomes significantly reduced, which would suggest that it would be much more susceptible to deformations. The biophysical implication of this would be the reduced ability of the RBC to recover its original biconcave shape, and hence in its deformed state this could potentially reduce the rate of oxygen uptake, at least in the short term. In an *in vivo* scenario, the concentration of alcohol would be far lower than those used in our experiment and it is likely that the RBC softening would be far less extreme in the same timescales. If alcohol is consumed chronically, it is likely that RBC *in vivo* will become less able to recover their initial elasticity, which could likely result in a reduction of overall oxygen uptake. However, we estimate that the amount of alcoholic consumption necessary for this effect to become apparent is far greater than typical levels consumed in the short term [35]. While it is likely that a change in membrane deformability is a component, other factors including a reduced RBC count and impaired RBC metabolism due to alcoholic presence are likely to be the primary cause of conditions such as anemia and other haematological afflictions [10, 36] .

4.3 Comparison to Similar Studies

The observation that both bending and shear moduli were affected by the presence of alcohol is in contrast with experiments in which the same *in vitro* microscopy technique is used as the one used in this study. Instead of alcohol, Hale *et al.* treated RBC with hydrogen peroxide (H_2O_2), and their analysis showed that the lower order modes ($n \leq 6$) were shifted downwards whereas higher order modes remained largely unaffected before and after treatment. This corresponded to an increase in the relative shear modulus and the membrane shear resistance, which is in contrast to our findings which show a decrease. The reason for this was thought to be spectrin-globin complex formation driven by oxidative stress [18]. While alcohols are known to cause oxidative stress [37], it is likely that the concentration of free radicals within the alcohol solutions in this experiment is not sufficient to induce oxidative stress on the membrane and lead to cytoskeleton stiffening.

5 Conclusions

Although at typical blood alcohol concentrations it is unlikely that alcohols contribute to a significant softening of the RBC membrane, we have shown that *in vitro* treatment of RBC with alcohols with concentrations in the regime 0.5-5% results in a more flexible lipid bilayer and a less rigid cell cytoskeleton. The extent to which softening occurs are more dramatic with increasing alcohol concentration and chain length, suggesting that the longer the hydrophobic region of the molecule, the more easily it penetrates and binds with the lipid bilayer. One of the most significant observations was that for longer chain alcohols, the shear modulus in particular experienced a significant reduction, with a near ten-fold decrease ($(11.7 \pm 4.9)\%$) at 5% methanol after just 10 minutes. This is indicative of a significant modification in the membrane confinement, which characterises a weakening of the spectrin network. Another notable finding was that of the cell enlargement, with a lack of any observational evidence of cells returning to their pre-treatment radius. The nature of the biophysical mechanism as to why this enlargement occured was largely unclear, hence further experimental research is needed to determine this. Applying the same methods to analyze the effects of longer chain alcohols on the membrane would give greater insight about how the size of a polar molecule affects its uptake into the membrane. A manifestation of this large reduction in membrane softening within humans could potentially lead to a loss of cell functionality, which could be a significant contributory factor in haematological conditions. Studying the effect of alcohols on RBC membranes can not only further our understanding of the interaction of the membrane with any general amphiphilic molecule, but could potentially have medical applications in technologies utilizing unilamellar vesicles.

6 Acknowledgements

I would like to personally thank my project supervisor Dr. Peter Petrov for the exceptional amount of support not just in the project, but also in being my personal academic tutor through a challenging past year. The clarity of his explanations, patience, hours of support and not least his overwhelming kindness have been exceptionally helpful to me. I would also like to extend my gratitude to my Father, Grandmother, Friends at the university and also to Bethan for their exceptional support and encouragement.

There once was a blood cell called Hillary
Who couldn't get through a capillary
"Oh no now I'm stuck
I'm all out of luck
Curse all those wretched distilleries!"

A Appendix

A.1 Definitions and Relations

The bending modulus, κ:

$$E_F = \frac{1}{2}\kappa \int_S (2H)^2 \, \mathrm{d}S \approx \frac{1}{2}\kappa \iint (\nabla^2 h(x,y))^2 \, \mathrm{d}x \, \mathrm{d}y$$

Surface tension coefficient, σ:

$$E_F = \frac{1}{2}\sigma \int_S \mathrm{d}S \approx \frac{1}{2}\sigma \iint (\nabla h(x,y))^2 \, \mathrm{d}x \, \mathrm{d}y$$

Confinement potential coefficient, γ:

$$E_F = \frac{1}{2}\gamma \int_S h(x,y)^2 \, \mathrm{d}S$$

Dimensionless moduli: $\tilde{\kappa}$, $\tilde{\sigma}$ and $\tilde{\gamma}$:

$$\tilde{\kappa} \equiv \frac{\kappa}{k_B T}$$

$$\tilde{\sigma} \equiv \frac{\sigma \langle R \rangle^2}{2\kappa}$$

$$\tilde{\gamma} \equiv \frac{\gamma \langle R \rangle^4}{\kappa}$$

Shear Modulus μ:

$$\mu = \frac{16\pi\kappa\sigma}{9k_B T}$$

$$\tilde{\mu} \equiv \frac{2\tilde{\kappa}\tilde{\sigma}}{\langle R \rangle^2}$$

$$\mu = \frac{32\pi k_B T}{9}\mu$$

N-octanol-water partition coefficient, P

$$P = \frac{c_{oct}^{S_i}}{c_{wat}^{S_i}}$$

Fluctuations occur at ambient conditions:

$$T = 295\mathrm{K}$$

$$p = 1.013 \times 10^5 \mathrm{Pa}$$

A.2 Coefficient values for Non Linear Fits

Fitting Coefficients for model function $f(n) = An^{-k}$ for the data given in Figure 5:

t/mins	A/ m^2	k
0	8.53×10^{-3}	4.34
10	3.43×10^{-3}	4.57
30	1.11×10^{-2}	4.02
90	3.41×10^{-3}	3.64

Fitting Coefficients for the model $f(t) = 100 - At^k e^{-t/\tau}$ for the data given in Figure 6a and Figure 6b:

Bending Modulus κ			
Alcohol	A/ mins^{-k}	k	τ / mins
Methanol	26.6	0.121	349
Ethanol	35.1	0.132	215
Propanol	37.3	0.096	75.4
Butanol	34.4	0.104	512
Shear Modulus μ			
Alcohol	A/ mins^{-k}	k	τ / mins
Methanol	21.9	0.132	175
Ethanol	35.1	0.141	113
Propanol	51.2	0.119	86.9
Butanol	47.4	0.145	228

Fitting Coefficients for the model $f(c) = 100e^{-\lambda c}$ for the data given in Figure 7a and Figure 7b:

Bending Modulus κ	
Alcohol	λ
Methanol	0.25
Ethanol	0.28
Propanol	0.57
Butanol	0.64
Shear Modulus μ	
Alcohol	λ
Methanol	0.29
Ethanol	0.29
Propanol	0.95
Butanol	0.92

Fitting Coefficients for the model $f(t) = 1+At^k e^{-t/\tau}$ for the data given in Figure 8a.

Alcohol	A/ mins^{-k}	k	τ / mins
Methanol	0.0230	0.121	349
Ethanol	0.0419	0.132	215
Propanol	0.0407	0.096	75.4
Butanol	0.0317	0.104	512

Fitting Coefficients for the model $f(c) = A(1/2 + (1 + \exp(-\lambda c + \delta))^{-1})$ for the data given in Figure 8b:

Alcohol	A	λ	δ
Methanol	0.73	0.45	1.97
Ethanol	0.71	1.86	2.31
Propanol	0.73	0.78	1.90
Butanol	0.72	1.40	2.16

Fitting Coefficients for the model $f(\log(P)) = A + B\log(P)$ for the data given in Figure 9:

Relative Modulus	A	B
Bending κ	59.1	12.2
Shear μ	52.8	24.1

References

[1] J. Gao, X. Dong, and Z. Wang, "Generation, purification and engineering of extracellular vesicles and their biomedical applications," *Methods*, vol. 177, pp. 114–125, 2020. Methods in Extracellular Vesicles and Mimetics.

[2] M. Sonmez, H. Y. Ince, O. Yalcin, V. Ajdžanović, I. Spasojević, H. J. Meiselman, and O. K. Baskurt, "The effect of alcohols on red blood cell mechanical properties and membrane fluidity depends on their molecular size," *PloS one*, vol. 8, no. 9, p. e76579, 2013.

[3] O. K. Baskurt, H. J. Meiselman, *et al.*, "Blood rheology and hemodynamics," in *Seminars in thrombosis and hemostasis*, vol. 29, pp. 435–450, Citeseer, 2003.

[4] *Amphiphiles*, ch. 4, pp. 161–220. John Wiley and Sons, Ltd, 2007.

[5] G. L. HW, M. Wortis, and R. Mukhopadhyay, "Stomatocyte–discocyte–echinocyte sequence of the human red blood cell: Evidence for the bilayer–couple hypothesis from membrane mechanics," *Proceedings of the National Academy of Sciences*, vol. 99, no. 26, pp. 16766–16769, 2002.

[6] D. Kunkel, "Red blood cells in a capillary, tem - stock image - c032/0832."

[7] N. Gov, A. Zilman, and S. Safran, "Cytoskeleton confinement and tension of red blood cell membranes," *Physical review letters*, vol. 90, no. 22, p. 228101, 2003.

[8] S. Chien, "Red cell deformability and its relevance to blood flow," *Annual review of physiology*, vol. 49, no. 1, pp. 177–192, 1987.

[9] S. R. Goodman, A. Kurdia, L. Ammann, D. Kakhniashvili, and O. Daescu, "The human red blood cell proteome and interactome," *Experimental Biology and Medicine*, vol. 232, no. 11, pp. 1391–1408, 2007.

[10] H. S. Ballard, "The hematological complications of alcoholism," *Alcohol health and research world*, vol. 21, no. 1, p. 42, 1997.

[11] D. Savage, J. Lindenbaum, *et al.*, "Anemia in alcoholics.," *Infection*, vol. 23, p. 19, 1986.

[12] J. Latvala, S. Parkkila, and O. Niemelä, "Excess alcohol consumption is common in patients with cytopenia: studies in blood and bone marrow cells," *Alcoholism: Clinical and Experimental Research*, vol. 28, no. 4, pp. 619–624, 2004.

[13] S. Maruyama, C. Hirayama, S. Yamamoto, M. Koda, A. Udagawa, Y. Kadowaki, M. Inoue, A. Sagayama, and K. Umeki, "Red blood cell status in alcoholic and non-alcoholic liver disease," *Journal of Laboratory and Clinical Medicine*, vol. 138, no. 5, pp. 332–337, 2001.

[14] B. Cylwik, M. Naklicki, E. Gruszewska, M. Szmitkowski, and L. Chrostek, "The distribution of serum folate concentration and red blood cell indices in alcoholics," *Journal of nutritional science and vitaminology*, vol. 59, no. 1, pp. 1–8, 2013.

[15] J. L. Deng, Q. Wei, M. H. Zhang, Y. Z. Wang, and Y. Q. Li, "Study of the effect of alcohol on single human red blood cells using near-infrared laser tweezers raman spectroscopy," *Journal of Raman Spectroscopy*, vol. 36, no. 3, pp. 257–261, 2005.

[16] H. I. Ingólfsson and O. S. Andersen, "Alcohol's effects on lipid bilayer properties," *Biophysical journal*, vol. 101, no. 4, pp. 847–855, 2011.

[17] H. V. Ly and M. L. Longo, "The influence of short-chain alcohols on interfacial tension, mechanical properties, area/molecule, and permeability of fluid lipid bilayers," *Biophysical Journal*, vol. 87, no. 2, pp. 1013–1033, 2004.

[18] J. P. Hale, C. P. Winlove, and P. G. Petrov, "Effect of hydroperoxides on red blood cell membrane mechanical properties," *Biophysical journal*, vol. 101, no. 8, pp. 1921–1929, 2011.

[19] K. M. Dubowski, "Stages of acute alcoholic influence/intoxication," *Police*, vol. 1, no. 3, p. 32, 1957.

[20] G. Marcelli, K. H. Parker, and C. P. Winlove, "Thermal fluctuations of red blood cell membrane via a constant-area particle-dynamics model," *Biophysical Journal*, vol. 89, no. 4, pp. 2473–2480, 2005.

[21] A. Zilker, M. Ziegler, and E. Sackmann, "Spectral analysis of erythrocyte flickering in the 0.3–4-μ m-1 regime by microinterferometry combined with fast image processing," *Physical Review A*, vol. 46, no. 12, p. 7998, 1992.

[22] J. Pécréaux, H.-G. Döbereiner, J. Prost, J.-F. Joanny, and P. Bassereau, "Refined contour analysis of giant unilamellar vesicles," *The European Physical Journal E*, vol. 13, no. 3, pp. 277–290, 2004.

[23] T. Auth, S. Safran, and N. S. Gov, "Fluctuations of coupled fluid and solid membranes with application to red blood cells," *Physical Review E*, vol. 76, no. 5, p. 051910, 2007.

[24] J. P. Hale, G. Marcelli, K. H. Parker, C. P. Winlove, and P. G. Petrov, "Red blood cell thermal fluctuations: comparison between experiment and molecular dynamics simulations," *Soft Matter*, vol. 5, no. 19, pp. 3603–3606, 2009.

[25] J. P. Hale, P. C. Winlove, and P. G. Petrov, 2011.

[26] J. Evans, W. Gratzer, N. Mohandas, K. Parker, and J. Sleep, "Fluctuations of the red blood cell membrane: relation to mechanical properties and lack of atp dependence," *Biophysical journal*, vol. 94, no. 10, pp. 4134–4144, 2008.

[27] R. C. Dorf, *Pocket book of electrical engineering formulas*. CRC Press, 2018.

[28] N. Gov and S. Safran, "Red blood cell membrane fluctuations and shape controlled by atp-induced cytoskeletal defects," *Biophysical journal*, vol. 88, no. 3, pp. 1859–1874, 2005.

[29] H. Yu and B. M. Wilamowski, "Levenberg-marquardt training," *Industrial electronics handbook*, vol. 5, no. 12, p. 1, 2011.

[30] R. Selvan, P. Parthasarathi, S. S. Iyengar, S. Ananthamurthy, and S. Bhattacharya, "Estimation of membrane bending modulus of stiffness tuned human red blood cells from micropore filtration studies," *PLOS ONE*, vol. 14, no. 12, p. e0226640, 2019.

[31] B. Fröhlich, J. Jäger, C. Lansche, C. P. Sanchez, M. Cyrklaff, B. Buchholz, S. T. Soubeiga, J. Simpore, H. Ito, U. S. Schwarz, *et al.*, "Hemoglobin s and c affect biomechanical membrane properties of p. falciparum-infected erythrocytes," *Communications biology*, vol. 2, no. 1, pp. 1–11, 2019.

[32] S. Amézqueta, X. Subirats, E. Fuguet, M. Rosés, and C. Ràfols, "Octanol-water partition constant," *Liquid-Phase Extraction*, pp. 183–208, 2020.

[33] C. Hansch, A. Leo, D. Hoekman, and D. Livingstone, *Exploring QSAR: hydrophobic, electronic, and steric constants*, vol. 48. American Chemical Society Washington, DC, 1995.

[34] S. C. McKarns, C. Hansch, W. S. Caldwell, W. T. Morgan, S. K. Moore, and D. J. Doolittle, "Correlation between hydrophobicity of short-chain aliphatic alcohols and their ability to alter plasma membrane integrity," *Fundamental and applied toxicology*, vol. 36, no. 1, pp. 62–70, 1997.

[35] ONS, "Ons dataset: Adult drinking habits in great britain," 2017.

[36] H. S. Ballard, "Alcohol, bone marrow, and blood," *Alcohol Research*, vol. 17, no. 4, p. 310, 1993.

[37] D. Wu and A. I. Cederbaum, "Alcohol, oxidative stress, and free radical damage," *Alcohol research & health*, vol. 27, no. 4, p. 277, 2003.

```
File: main.tex
Encoding: utf8
Sum count: 7540
Words in text: 6260
Words in headers: 67
Words outside text (captions, etc.): 810
Number of headers: 23
Number of floats/tables/figures: 16
Number of math inlines: 380
Number of math displayed: 23

(errors:2)
```